

Original Article

Separation of β -amyloid binding and white matter uptake of ^{18}F -flutemetamol using spectral analysis

Kerstin Heurling¹, Christopher Buckley², Rik Vandenberghe³, Koen Van Laere⁴, Mark Lubberink^{1,5}

¹Department of Surgical Sciences, Uppsala University, Uppsala, Sweden; ²GE Healthcare, Amersham, UK; ³Department of Neurosciences, KU Leuven and University Hospitals Leuven, Leuven, Belgium; ⁴Department of Imaging and Pathology, KU Leuven and University Hospitals Leuven, Leuven, Belgium; ⁵Medical Physics, Uppsala University Hospital, Uppsala, Sweden

Received July 31, 2015; Accepted August 26, 2015; Epub October 12, 2015; Published October 15, 2015

Abstract: The kinetic components of the β -amyloid ligand ^{18}F -flutemetamol binding in grey and white matter were investigated through spectral analysis, and a method developed for creation of parametric images separating grey and white matter uptake. Tracer uptake in grey and white matter and cerebellar cortex was analyzed through spectral analysis in six subjects, with (n=4) or without (n=2) apparent β -amyloid deposition, having undergone dynamic ^{18}F -flutemetamol scanning with arterial blood sampling. The spectra were divided into three components: slow, intermediate and fast basis function rates. The contribution of each of the components to total volume of distribution (V_T) was assessed for different tissue types. The slow component dominated in white matter (average 90%), had a higher contribution to grey matter V_T in subjects with β -amyloid deposition (average 44%) than without (average 6%) and was absent in cerebellar cortex, attributing the slow component of ^{18}F -flutemetamol uptake in grey matter to β -amyloid binding. Parametric images of voxel-based spectral analysis were created for V_T , the slow component and images segmented based on the slow component contribution; confirming that grey matter and white matter uptake can be discriminated on voxel-level using a threshold for the contribution from the slow component to V_T .

Keywords: Alzheimer's, positron emission tomography, kinetic modelling, white matter disease, molecular imaging

Introduction

Since its introduction in the early 21st century, amyloid imaging has been of great interest both in clinical research of the pathogenesis of Alzheimer's disease (AD) and in clinical practice given its ability to detect aggregates of β -amyloid in the cerebral cortex, a pathological hallmark of AD. Subsequent to the introduction of what is arguably the most studied amyloid imaging agent, the ^{11}C labelled Pittsburgh Compound B (^{11}C -PIB) [1], three ^{18}F labelled alternative tracers were developed to exploit the benefits of a longer radioactive half-life and have been approved by regulatory authorities for clinical use: ^{18}F -florbetapir, ^{18}F -florbetaben and ^{18}F -flutemetamol. The latter is a structural analogue of ^{11}C -PIB, and both ^{11}C -PIB and ^{18}F -flutemetamol are analogues of Thioflavin T, a histochemical dye for fibrillar β -amyloid.

Compared to ^{11}C -PIB, the ^{18}F labelled amyloid imaging tracers typically have a higher uptake

in subcortical white matter of the brain, in spite of this tissue not being affected by β -amyloid deposits in AD pathology [2]. The uptake in white matter is similar in healthy subjects and patients with AD [3]. In qualitative analyses, i.e. visual assessments, of β -amyloid imaging, the characteristic white matter pattern can in fact be useful in the discrimination of the uptake pattern typical of an AD patient from the normal uptake pattern in a subject without β -amyloid deposition [4]. It may, however, affect semi-quantitative standardized uptake value ratio (SUVR) analyses due to partial volume effects (PVE) [5]. The underlying mechanism of the uptake in white matter of β -amyloid imaging agents has been debated. For fluorine-18 agents, it has been suggested to be related to increased tracer lipophilicity [6] and as such to be due to non-specific uptake unrelated to binding of the tracer to a specific target protein. For ^{11}C -PIB the uptake in white matter was shown to be non-specific in vitro and in vivo [7], but it has also been hypothesized that the binding of

^{11}C -PIB to white matter is due to specific binding to β -sheet structured myelin basic protein, correlating with the mRNA expression of myelin proteins [8] and as such can be useful for identifying lesions in the white matter in multiple sclerosis [9] as well as in age-associated demyelination where a significantly lower ^{11}C -PIB uptake has been seen in white matter lesions compared to normal appearing white matter [10].

Though some efforts have been made to study the white matter binding of ^{11}C -PIB, there have been no reports of attempts to characterize the mechanism of binding of ^{18}F -flutemetamol in white matter and whether it can be distinguished from grey matter binding through kinetic modelling. Spectral analysis has been shown to have higher sensitivity for quantification of ^{11}C -PIB than traditional kinetic modelling [11] but has not been previously applied to ^{18}F -flutemetamol. Our aims of this study were therefore in three parts: 1) to identify the components of ^{18}F -flutemetamol binding both in grey matter - affected and non-affected by β -amyloid deposition - and in white matter through spectral analysis, 2) to investigate the impact of PVE on the kinetic modeling of ^{18}F -flutemetamol by means of simulations and 3) to attempt to develop methods for creating parametric images that can separate tracer uptake due to binding to β -amyloid deposits and binding in white matter.

Materials and methods

Subjects and data acquisition

Data from a previously published study [12, 13] including six subjects scanned dynamically with ^{18}F -flutemetamol, were analyzed post-hoc in order to address our study aims. Three were healthy volunteers (HV); one male and two females (mean age, range: 62, 56-71) with a Mini-Mental State Examination (MMSE) scoring between 28 and 30 and a Clinical Dementia Rating of 0. Three subjects had a diagnosis of early-stage clinically probable AD; all were males (mean age, range: 62, 55-68). The AD subjects had to fulfill the criteria of the National Institute of Neurological and Communicative Disorders and Stroke and of the Alzheimer's Disease and Related Disorders Association for clinically probable AD as well as the DSM-IV criteria for dementia of Alzheimer's

type. The inclusion criteria for AD patients included a MMSE between 18 and 26 and a Clinical Dementia Rating between 0.5 and 2. The included AD subjects had MMSE scoring between 22 and 24, for more detailed information on the neuropsychology testing see Nelissen et al., 2009. All participants provided their written informed consent in accordance with the Declaration of Helsinki and the study protocol was approved by the Ethical Committee of the University Hospitals Leuven.

Each subject underwent a high-resolution T1-weighted MRI examination, performed on a 1.5 T *Intera* scanner (Philips, Guildford, Surrey, UK). The scan was used as part of screening to exclude subjects with structural abnormalities, for region definition and segmentation in the PET data processing. PET examinations were performed on a *Biograph* PET/CT (Siemens, Erlangen, Germany) in 3D list mode starting from time of administration of a target dose of 185 MBq Flutemetamol F18 Injection to 90 min post administration. The PET data were reconstructed into 25 frames (4×30, 6×60, 4×180, 8×300 sec) using Fourier re-binning, 2D ordered subsets expectation maximization and a Gaussian filter with a FWHM of 5 mm resulting in an image resolution of approximately 7 mm. The reconstruction included all the appropriate corrections such as for attenuation, randoms and scatter.

Arterial blood samples were collected for radioactivity measurements in whole blood and plasma, every 10 sec during the first minute, every 15 sec up to 3 minutes and at 4, 8, 15, 30, 45, 60 and 90 min post injection. Arterial samples were also collected at 2, 5, 20, 60, 180 and 240 min for determination of fraction of radioactive parent compound and metabolites. From these data a metabolite-corrected plasma input curve was created and used for spectral analysis of ^{18}F -flutemetamol.

A previously published analysis of the data has shown that one of the healthy volunteers showed an increased uptake [12], potentially indicative of pre-clinical AD. For the purpose of these analyses, correlations between clinical status and evident ^{18}F -flutemetamol retention were not the main objective, as the tracer binding properties on a kinetic level are independent of the cognitive status of the subject. Instead, where relevant, the subjects were

compared based on their ^{18}F -flutemetamol retention status, resulting in four subjects with AD typical uptake pattern ("positive subjects", subjects P1-P4), and two subjects with control typical uptake pattern ("negative subjects", subjects N1 and N2), as defined by subsequent studies [3, 14].

Image processing and spectral analysis

The dynamic PET data were corrected for inter-frame movements [15] using VOIager4 (GE Healthcare, Uppsala, Sweden). MRI images were co-registered to the PET images by means of an early summation image of frames 2-10 (30 sec to 8 min p.i) resembling a flow image with maximal cortical information. The co-registrations were performed using Statistical Parametric Mapping (SPM5; Wellcome Trust Center for Neuroimaging, University College London, UK). Volumes of interest (VOI) were defined using a probabilistic VOI template in PVE lab software based on each individual MRI [16]. VOIs were then applied to the dynamic PET data generating mean time-activity curves (TACs) for 16 grey matter regions averaged over the left and right hemispheres (superior frontal cortex, medial inferior frontal cortex, orbital frontal cortex, dorsolateral prefrontal cortex, ventrolateral prefrontal cortex, superior temporal cortex, medial inferior temporal cortex, insula, parietal cortex, thalamus, sensory motor cortex, occipital cortex, putamen, caudate, anterior cingulate cortex and posterior cingulate cortex), the total grey matter, total white matter and cerebellar cortex with and without partial volume effects correction (PVC) using the modified Müller-Gärtner method in PVE lab [17].

The kinetic components of ^{18}F -flutemetamol uptake were analyzed using spectral analysis for the TACs with and without PVC. Spectral analysis is a data-driven method characterizing the impulse response function (IRF) as a sum of exponential terms, fitting a set of k basis functions to the data, without restriction of a predefined compartmental model. V_T is then estimated as a function of the IRF [18] which is given by the following equation

$$IRF(t) = \sum_{i=1}^k \alpha_i \cdot e^{-\beta_i t}$$

Fifty basis functions were used with predetermined β logarithmically distributed between 0.0111 min^{-1} (equal to $1/T$ where T is the scan-

ning duration 90 min) and 2 min^{-1} , returning the peak height α_i [19]. β_i corresponds to k_2 and α_i to K_1 in a compartment model IRF and thus providing a contribution to V_T of each of the 50 basis functions and estimating V_T as the area under the IRF curve. The basis functions were divided into categories based on peak distribution across all subjects. The distribution volume for each category was estimated as $V_j = \sum \alpha_j / \beta_j$, where $j=A, B, \dots, X$, of the basis functions within each of the X categories, as well as the percentage contribution of each V_j to the total V_T ($\%V_j$). Differences in grey and white matter properties were identified, and used as a method for potential discrimination of uptake type in the creation of parametric images. Effects of PVE on the estimated V_T and contribution of respective component to V_T were assessed using Student's t-test.

The binding potential (BP_{ND}) in each of the 16 grey matter regions was estimated through an indirect plasma input 2-tissue compartment model, calculating BP_{ND} as the distribution volume ratio (DVR)-1 using cerebellar cortex as reference region. The correlation between the spectral analysis and 2-tissue compartment model estimates was assessed.

Simulation of partial volume effects

The impact of PVE on the quantification of ^{18}F -flutemetamol uptake was investigated through simulations. Digital phantom scans were created by using grey/white matter segmented MR images from a representative negative and a positive subject, assuming homogeneous tracer uptake within grey and white matter and cerebellar cortex. While this assumption is not supported in reality, especially where the uptake differs with respect to presence of β -amyloid deposits in grey matter, it was assumed sufficient for the evaluation of PVE. Characteristics of tracer uptake were based on plasma input functions and kinetic parameters of the three tissue types from the spectral analysis performed in the two subjects. PVE were introduced by applying smoothing using a Gaussian point spread function of 7 FWHM on the digital phantom. Recovery of the uptake in the three tissue types was estimated through comparison of each tissue type before and after smoothing. TACs were generated for the original and smoothed digital phantom and quantified using spectral analysis [18].

Spectral analysis of ^{18}F -flutemetamol

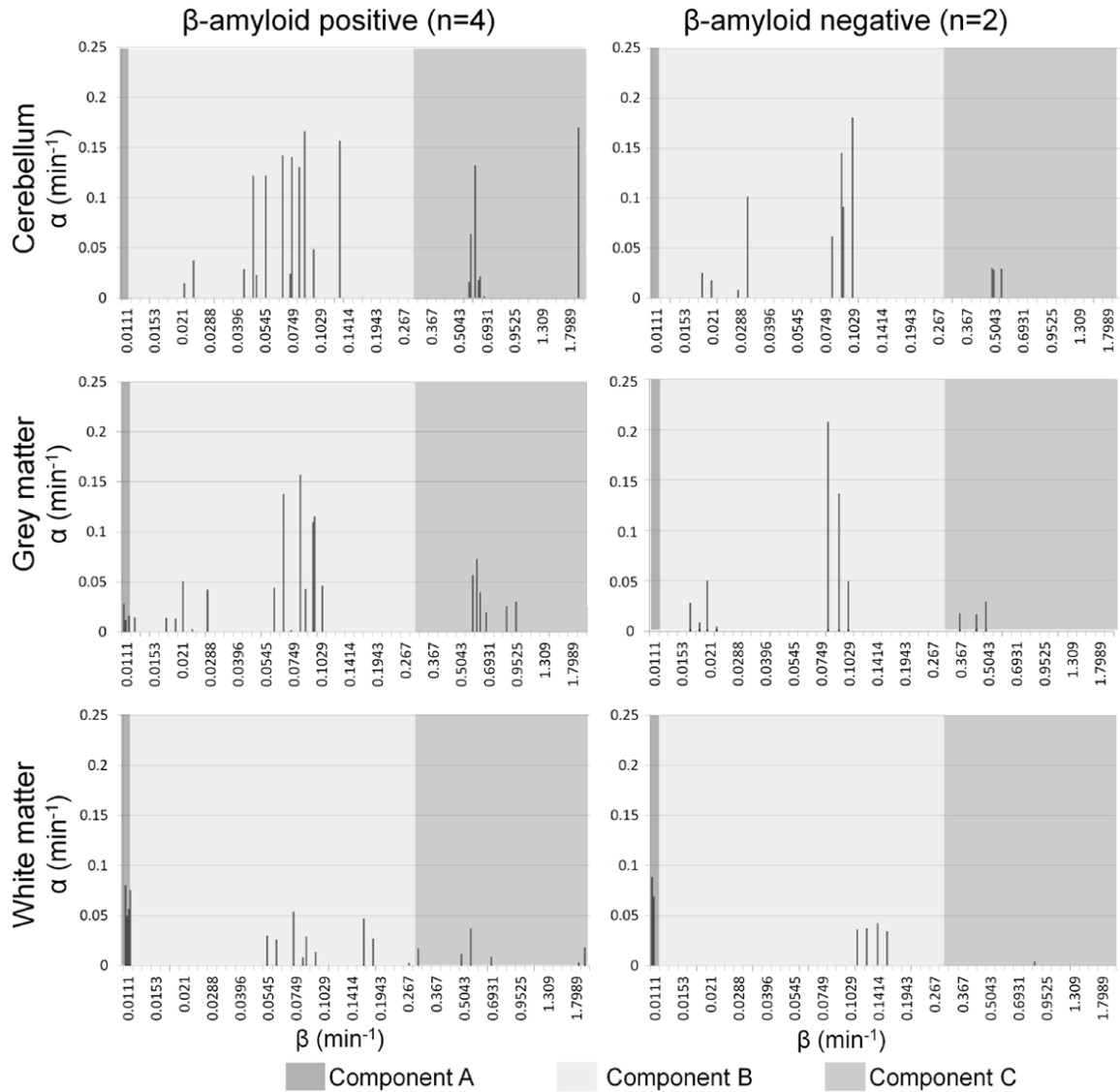


Figure 1. Spectral analysis peaks of (from top to bottom) ^{18}F -flutemetamol uptake in cerebellar cortex, total grey and total white matter. Left column: the combined peaks of four subjects with positive uptake profile, right: the combined peaks of two subjects with negative uptake profile. The dark grey boxes on the left of each graph represent the range of peaks included in the slow component A ($\beta \leq 0.0111 \text{ min}^{-1}$), the light grey boxes show the intermediate range B ($\beta: 0.0124\text{-}0.1748 \text{ min}^{-1}$), and the grey on the right of each graph represent the fast component range C ($\beta: 0.267\text{-}2 \text{ min}^{-1}$). The slow component is completely absent in cerebellar cortex, and in the grey matter of negative subjects, while present in the grey matter of positive subjects and dominating in the white matter of both positive and negative subjects.

The effects of PVE on the positive and negative phantoms were assessed by comparison of the spectral analysis estimates from the original and smoothed data.

Parametric images

Parametric images were created using voxel-based spectral analysis with five basis functions, with β logarithmically spaced between 0.0111 and 2 min^{-1} . The number of basis func-

tions was limited to five in order to decrease processing time and the simplification was validated by applying the VOI maps onto the parametric V_T images. Regionally averaged V_T values were obtained and compared with those from the VOI-based spectral analysis using 50 basis functions. Using the V_T of the cerebellar grey matter region, DVR-1 was estimated for each region and compared to BP_{ND} estimates from a parametric basis function implementation of the simplified reference tissue model

Spectral analysis of ^{18}F -flutemetamol

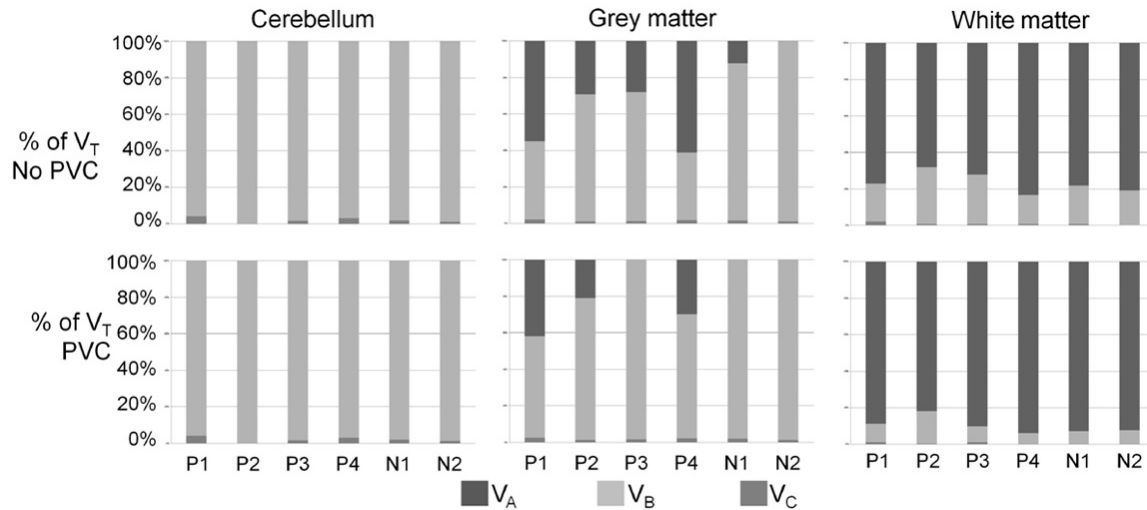


Figure 2. Contribution of kinetic components to V_T before and after partial volume effects correction (PVC). Subjects P1-P4 are the four positive subjects, N1 and N2 the negative subjects. Top row: before PVC, bottom row: after PVC. Slow component A presented in dark grey, intermediate component B presented in light grey and fast component C presented in grey.

(SRTM), called RPM [20, 21] previously validated for creation of parametric images of ^{18}F -flutemetamol [22].

Using the unique properties of grey matter and white matter as identified by the VOI-based spectral analysis, voxels were classified as typical grey matter or white matter and two parametric images for each subject were created, one including only the voxels classified as grey matter and one including only voxels classified as white matter. For each unique voxel, the V_T was estimated in each respective parametric image. In addition, a parametric image containing the kinetic component V_j hypothesized to be typical for white matter uptake and specific binding to β -amyloid in grey matter in the both in all voxels and in voxels classified as grey matter was created for each subject.

Results

Spectral analysis of ^{18}F -flutemetamol uptake

Three main categories of exponential components were identified, both in amyloid-negative and positive subjects. The categories were defined, slowest to fastest, as A: $k_2 \leq 0.0111 \text{ min}^{-1}$, B: k_2 ranging from 0.0124 to 0.1748 min^{-1} and C: k_2 ranging from 0.267 to 2 min^{-1} , with V_A , V_B and V_C being the volume of distribution of each component. Combined spectra for

positive and negative subjects are shown in **Figure 1**.

In white matter and cerebellar cortex, the contribution of the components to V_T did not differ between the negative and positive subjects. In cerebellum, the slow component A was not detected, component B was dominant ($\%V_B = 97.7\% \pm 1.1$), and component C had the remaining minor contribution when data had undergone PVC. Correcting the uptake for PVE increased the V_T in cerebellar cortex by $14\% \pm 0.4$ ($p < 0.001$), but did not affect the relative contribution of the different components, i.e. also without PVC component B represented the entire V_T .

In white matter, component A was dominating ($\%V_A = 90.0\% \pm 4.4$ to total V_T), followed by component B ($\%V_B = 9.6\% \pm 4.2$) and negligible contribution from component C ($\%V_C = 0.4\% \pm 0.6$) when data was corrected for PVE. PVC had no significant effect on V_T in the white matter, however $\%V_A$ increased ($p < 0.001$) and $\%V_B$ decreased ($p < 0.001$) compared to uncorrected data.

After PVC, component A was absent in the grey matter of two negative subjects, and $\%V_B$ was approximately 100%, similar to cerebellar cortex. In the grey matter of three of the four positive subjects, $\%V_A$ ranged between 21 and 42%,

Spectral analysis of ¹⁸F-flutemetamol

Table 1. Mean kinetic parameters of region based spectral analysis

No correction for PVE		Component			Corrected for PVE		Component		
K ₁	Total K ₁	A	B	C	Total K ₁	A	B	C	
Negative					Negative				
Grey matter	0.24	0.00	0.21	0.03	Grey matter	0.28	0.00	0.24	0.03
White matter	0.22	0.06	0.14	0.02	White matter	0.16	0.08	0.07	0.00
Cerebellar cortex	0.30	0.00	0.26	0.04	Cerebellar cortex	0.36	0.00	0.32	0.04
Positive					Positive				
Grey matter	0.24	0.03	0.16	0.05	Grey matter	0.27	0.02	0.20	0.06
White matter	0.22	0.06	0.12	0.05	White matter	0.15	0.07	0.06	0.02
Cerebellar cortex	0.33	0.00	0.24	0.09	Cerebellar cortex	0.39	0.00	0.30	0.05
V _T	V _T	V _{TA}	V _{TB}	V _{TC}	V _T	V _{TA}	V _{TB}	V _{TC}	
Negative					Negative				
Grey matter	4.89	0.33	4.49	0.07	Grey matter	4.67	0.00	4.60	0.07
White matter	7.30	5.80	1.47	0.03	White matter	7.64	7.09	0.52	0.00
Cerebellar cortex	4.80	0.00	4.73	0.07	Cerebellar cortex	5.43	0.00	5.35	0.08
Positive					Positive				
Grey matter	5.06	2.27	2.71	0.08	Grey matter	5.04	1.26	3.68	0.09
White matter	6.76	5.12	1.57	0.08	White matter	6.63	5.91	0.69	0.03
Cerebellar cortex	4.01	0.00	3.90	0.11	Cerebellar cortex	4.57	0.00	4.44	0.13
%V _x of V _T	%V _A	%V _B	%V _C		%V _A	%V _B	%V _C		
Negative					Negative				
Grey matter		6.1	92.5	1.4	Grey matter		0.0	98.4	1.5
White matter		79.6	20.1	0.4	White matter		92.7	7.3	0.0
Cerebellar cortex		0.0	98.6	1.5	Cerebellar cortex		0.0	98.5	1.5
Positive					Positive				
Grey matter		43.4	55.1	1.6	Grey matter		23.2	75.0	1.8
White matter		75.2	23.8	1.1	White matter		88.7	10.7	0.4
Cerebellar cortex		0.0	97.3	2.7	Cerebellar cortex		0.0	97.3	2.7

Negative: mean of the two subjects with amyloid negative uptake pattern; Positive: mean of the four subjects with amyloid positive uptake pattern; K₁: unidirectional clearance from blood to tissue, sum of α_j across all β_j or within each component A, B and C; V_T: total volume of distribution.

whereas it was zero in subject P3. The contribution of the different components to V_T in the three tissue types is shown visually in **Figure 2**, before and after PVC. PVC had the opposite effect on grey matter uptake compared to white matter, %V_A decreased (and was removed completely in two subjects, p=0.03) and the %V_B increased (p=0.03). No significant change in V_T was observed.

Magnitude of K₁, V_T and the component contribution in grey matter, white matter and cerebellar cortex uptake with and without PVC are listed in **Table 1**.

Spectral analysis estimates of DVR-1 in 16 grey matter VOIs, using cerebellar cortex as reference region, correlated well with 2-tissue com-

partment model DVR-1 estimates (Pearson's r=0.98, slope=1.04) for data uncorrected for PVE are shown in **Figure 3A**.

Discrimination of tissue types

A threshold for discrimination of grey and white matter based on VOI estimates of the %V_A in data uncorrected for PVE was identified by locating the exact midpoint between white matter and grey matter mean estimates expressed in standard deviations (SD):

$$\text{Threshold} = \overline{\%V_A^{WM}} - \frac{\overline{\%V_A^{WM}} - \overline{\%V_A^{GM}}}{SD^{WM} + SD^{GM}} \cdot SD^{WM}$$

The threshold estimated was 0.69, i.e. if the %V_A is higher than 69%, the data should be classified as coming from white matter.

Spectral analysis of ^{18}F -flutemetamol

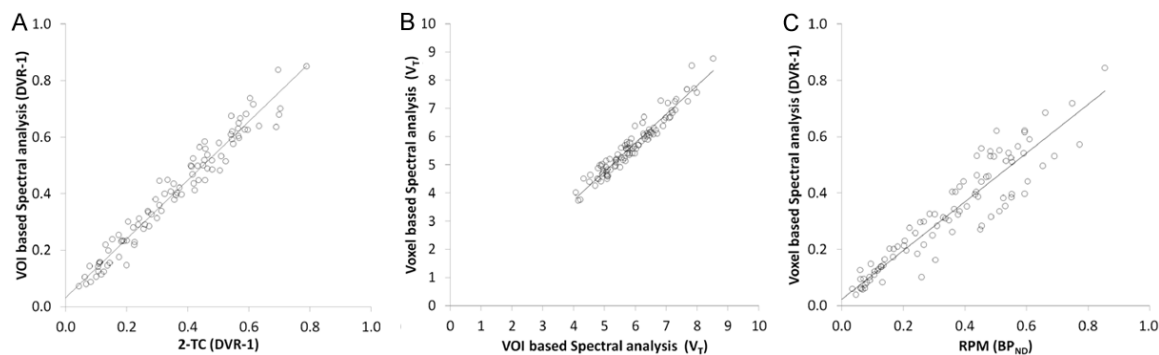


Figure 3. Correlation plots of methods for quantification. (A) VOI-based spectral analysis DVR-1 vs plasma input 2-tissue compartment model DVR-1 ($r=0.98$), (B) Voxel-based spectral analysis DVR-1 using five basis functions vs VOI-based spectral analysis DVR-1 using 50 basis functions ($r=0.97$) and (C) voxel-based spectral analysis DVR-1 vs RPM BP_{ND} ($r=0.93$).

Simulation of partial volume effects

The simulation study demonstrated that after smoothing was applied to mimic PVE, the recovery in a positive phantom was 64% in grey matter, 68% in white matter and 79% in cerebellar cortex. In a negative phantom, the recovery was 68% in grey matter, 71% in white matter and 77% in cerebellar cortex, i.e. very similar to that of the positive phantom.

The V_T in grey matter was reduced 21% in the positive phantom, but decreased with only 6% in the grey matter of a negative phantom as an effect of the simulated PVE. The V_T in white matter was less affected by PVE in the positive phantom (7% decrease) and in the negative phantom the white matter V_T decreased with 12%. V_T in cerebellar cortex decreased with 5% in the positive phantom and 9% in the negative phantom. As a result, the DVR using cerebellar cortex as reference region decreased in the grey matter with 17% in the positive phantom but only 4% in the negative phantom, while the white matter DVR increased with 17% in the positive phantom and decreased with 10% in the negative phantom.

On a component level, the $\%V_A$ increased from 38 to 44% in grey matter of the positive phantom, and from 0 to 32% in the negative phantom. In white matter the $\%V_A$ decreased from 82 to 71% in the positive phantom, and from 92 to 81% in the negative phantom.

Parametric images

Starting with the optimal threshold for contribution of component A to V_T as classifier of each

voxel, the voxels with $\%V_A \geq 69\%$ were assigned to the white matter parametric image, and $\%V_A < 69\%$ were assigned to the grey matter parametric image. For adaptation of the region based threshold to voxel-based analysis, which is more sensitive to PVE especially on the border between grey and white matter, iterations of thresholds starting with the estimated threshold was made returning an optimal threshold that did not over-classify grey matter voxels as white matter or vice versa as compared to the MRI. Two iterations of lower thresholds were tested $\%V_A = 60\%$ and $\%V_A = 50\%$, where the latter instead was shown to classify white matter voxels in grey matter affected by β -amyloid accumulation. Five parametric images were created:

- V_T - voxel-based spectral analysis in all voxels
- V_A - voxel-based V_T of component A in all voxels
- V_T^{GM} - voxel-based spectral analysis in voxels with $\%V_A < 60\%$ (grey matter voxels)
- V_T^{WM} - voxel-based spectral analysis in voxels with $\%V_A \geq 60\%$ (all voxels)
- V_A^{GM} - V_T of component A in voxels with $\%V_A < 60\%$ (grey matter voxels)

Examples of V_T , V_A , V_T^{GM} , V_T^{WM} and V_A^{GM} are shown in **Figure 4** for a representative negative and positive subject. V_T^{WM} showed a distinct white matter pattern in the negative subject, whereas in the positive subject it was in part slightly distorted due to atrophy. The signal

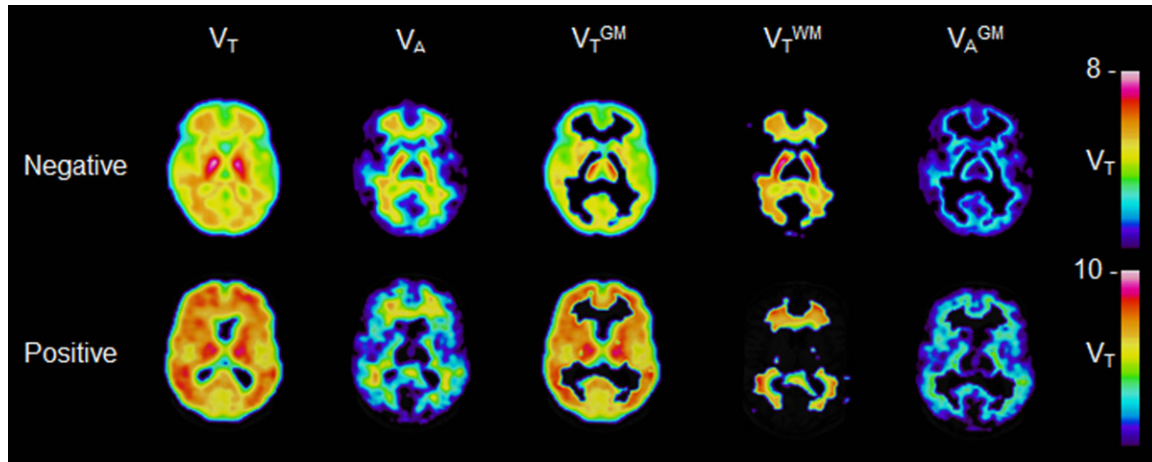


Figure 4. Parametric spectral analysis images. Top row: negative subject N2 (MMSE=29) and bottom row: positive subject P2 (MMSE=23). Maximum intensity in all images is set to twice the V_T in cerebellar grey matter of respective subject.

from component A in grey matter, as seen in the V_A^{GM} image showed a halo of high uptake outlining the white matter border in the negative subject, while the higher uptake spread out in the cortical parts in the positive subject.

The V_T of the 16 grey matter regions and cerebellar cortex from voxel-based spectral analysis using 5 basis functions demonstrated a high correlation with the V_T from VOI-based spectral analysis using 50 basis functions without PVC, with Pearson's $r=0.97$ and a slope of 0.99 (**Figure 3B**). There was a significant correlation between the voxel-based estimation of DVR-1 using cerebellar cortex as reference region and V_A across subjects and regions (Pearson's $r=0.68$, $p<0.0001$). The voxel-based DVR-1 also correlated well across all subjects with voxel-based BP_{ND} from RPM (Pearson's $r=0.93$, slope=0.85) (**Figure 3C**).

Discussion

Previous studies have quantified ^{18}F -flutemetamol uptake by means of either compartment modelling, graphical analysis or semi-quantitatively using the target to reference ratio, SUVR. The present work investigated whether spectral analysis could be applied for quantitation of uptake, as well as for separation of grey and white matter uptake.

Uptake of ^{18}F -flutemetamol as quantified by spectral analysis correlated well with quantitation through arterial input compartment model-

ing, which is considered the gold standard in PET quantitation. Spectral analysis of PVC data demonstrated the presence of three main components in the uptake of ^{18}F -flutemetamol, ranging from very slow (irreversible or near irreversible) and intermediate to fast. The contribution of the fast component was minor overall and independent of whether the subject exhibited an AD or control typical uptake pattern, and was likely due to dispersion or noise in the input function [18]. It cannot be concluded from this study whether the intermediate and fast reversible components represent parallel compartments, a result of a heterogeneous tissue, or catenary.

The components dominating the contribution to the total uptake varied between the different types of tissues studied. In white matter, the slow component had the major contribution to the total uptake, whereas in the cerebellar cortex, this slow component was completely absent and instead the intermediate component had the major contribution to the total uptake, representing non-specific reversible binding. This was consistent across all six subjects studied, indicating that non-specific binding in grey matter, such as the uptake in the cerebellar cortex, has different kinetic properties than the binding in white matter, assumed to be non-specific. While the basis function with slowest kinetics in spectral analysis may include irreversible kinetics, the uptake in white matter could not be described well by an irreversible 2-tissue compartment model implying

Spectral analysis of ^{18}F -flutemetamol

that the binding in white matter was in fact of reversible, although very slow.

The dominating slow component of ^{18}F -flutemetamol in white matter was not in line with the kinetics of the analogue tracer ^{11}C -PIB, which exhibits only a fast component in white matter when analyzed with spectral analysis [23]. This may be a consequence of the higher lipophilicity of ^{18}F -flutemetamol compared to its ^{11}C analogue.

In grey matter the slow component appeared to evince the presence of β -amyloid: two of the AD subjects and the control subject with a positive uptake pattern had a contribution of the slow component. In contrast, the slow component was absent in the remaining two controls and the dominating contribution to the uptake was the intermediate component, similar to the uptake in cerebellar cortex. The slow component was also missing in the grey matter of one of the positive AD subjects after correction for PVE.

Without PVC, the neighboring tissue contaminated the signals in white and grey matter; the slow component was present in all positive scans, and to a smaller extent in one of the negative scans. The contribution to V_T of the slow component in the positive AD subject where spectral analysis of the PVC data had failed to detect the slow component, was on similar level as the other positive subjects, while it was much lower in the negative subjects. This suggests that the PVC may have removed the actual signal, explaining the absence of the slow component in the positive AD subject.

The intermediate component was also more prominent in the white matter, but the slow component contribution was still larger than within grey matter tissue. This was not seen for the cerebellar cortex however, in which the slow component was still completely absent supporting the assumption that the cerebellar cortex exhibits a 1-tissue compartment kinetics and its appropriateness as reference region [12]. The volume of distribution of the slow component of regional voxel-based analysis correlated with the regional voxel-based DVR-1. The same pattern was observed for ^{11}C -PIB where one of the slower components varied linearly with the Logan V_T in AD subjects but not in controls [23].

Sensitivity of spectral analysis has been indicated especially in data with high noise, and for the low rate basis functions [19], where effects on component detection resulting in shifting of components as well as detection of false components in the system would occur. Bias-correction utilizing bootstrapping has been shown to lower the bias, but at the cost of an increasing variance [19]. Another approach is to apply numerical filtering [18] where coefficients below a certain cutoff frequency β_{cutoff} are summed, to compensate for noise in the data. The analyses included here focused on total grey matter, total white matter and the cerebellar cortex. The size of the two former produces data with low noise especially for the high uptake in the grey matter of amyloid-positive subjects and the white matter of all subjects. In the regions with lower counts and higher noise, cerebellar cortex and grey matter of amyloid negative subjects, the slow component was not detected. Nor were any peaks detected near the limit that could indicate that a shift of the components had taken place. In our analysis, the basis function with lowest rate were defined as $\beta \leq 0.0111 \text{ min}^{-1}$ or $1/T$ where T is the end time of the scanning interval [24]. This corresponds in effect to numerical filtering [18]. This definition of the lowest rate basis function does not allow for separation of reversible and irreversible kinetics, but previous analyses using compartment modeling has shown that the kinetics is best described by reversible models [12].

Our simulation studies confirmed the clinical findings with respect to impact of PVE on the quantification of ^{18}F -flutemetamol uptake, showing an increase in the grey matter of the slow kinetic component and a decrease in the white matter. Specifically in the negative digital phantom, the contribution increased from 0 to 32%, but the DVR only increased 4% suggesting that while spillover from white matter does contaminate the signal in grey matter, the impact on the absolute quantification is minor. Some limitations of the simulation study were that we assumed uniform uptake within each tissue type which is not in line with reality, and the analysis was limited to only one digital phantom per uptake category. However, in spite of these limitations the simulations still work as an objective observation of the impact of PVE.

In order to decrease the noise in the voxel-based spectral analysis, only 5 basis functions

were used. The slow component, which was of highest importance for the discrimination between grey and white matter kinetics was defined similarly in both VOI- and voxel-based analyses and the correlation between the V_T estimates from VOI and voxel-based spectral analysis was excellent. While the method of discrimination between white and grey matter kinetics was based on uptake in the global grey and white matter and not taking into account the PVE or the higher relative noise in voxel-based activity measurements, the separation of the tissue types was successful. Previous studies using traditional plasma input compartment modelling have not been able to discriminate between the specific binding of ^{18}F -flutemetamol to β -amyloid, and the high non-specific binding in white matter [12].

When reviewing the contribution of the slow component in the grey matter of negative subjects with control typical uptake pattern, white matter uptake spills over into the grey matter voxels due to PVE, for which the image data had not been corrected, resulting in a higher signal outlining the excluded white matter classified voxels. The evident PVE were only visible directly adjacent to the white matter and not further out in the lateral cortex, as expected from PVE. Among the positive subjects with AD typical uptake pattern, a higher V_T of slow component was also detected in the cortex, however, with a larger spread than that seen in negative subjects. PVE could be decreased by using a lower threshold of contribution from slow component to V_T for classifying voxels as white matter, thus expanding the volume classified as white matter, but at the risk of classifying grey matter voxels with specific binding to β -amyloid as white matter instead.

The similar kinetic properties for the specific binding of ^{18}F -flutemetamol to β -amyloid in grey matter, and non-specific binding in white matter, could in fact reveal binding to β -sheet structured myelin basic protein in white matter even more prominent than that proposed for ^{11}C -PIB which could result in even larger decrease in uptake in demyelinated lesions than for ^{11}C -PIB [9, 10]. It remains to be investigated whether the findings in these previous studies are related to blood flow alterations in studied lesions, as neither applied kinetic modelling in their quantification. Spectral analysis would constitute an attractive method for quantification in potential future studies aiming to investigate uptake in white matter lesions using

^{18}F -flutemetamol since the specific binding represented by the slow component can be quantified, as described here. Further *in vitro* studies are required to investigate whether the high white matter uptake is due to the lipophilicity of ^{18}F -flutemetamol or specific binding.

Conclusions

Using spectral analysis, three main kinetic components could be identified in the uptake of ^{18}F -flutemetamol. Specific binding of ^{18}F -flutemetamol to β -amyloid was characterized by presence of a slow kinetic component, which also dominated the white matter uptake. Using voxel-based spectral analysis, grey matter and white matter voxels could be discriminated using a threshold for the level of contribution from the slowest component to the total volume of distribution.

Acknowledgements

The authors would like to express their gratitude to the participating volunteers, patients and their families. We would also like to thank the staff at KU Leuven and GE Healthcare for all the work in the original Phase I study, and for making the data available for this study. The study was designed and sponsored by GE Healthcare. Ms Heurling is a former employee of GE Healthcare, Dr Buckley is an employee of GE Healthcare. Dr Vandenberghe was principal investigator and Dr Van Laere was co-investigator in the original GE Healthcare sponsored Phase I study.

Disclosure of conflict of interest

The image data utilized for this study were part of a GE Healthcare sponsored clinical trial. The primary study objectives have been published elsewhere, and this manuscript presents an independent exploratory post hoc analysis.

Address correspondence to: Kerstin Heurling, Department of Surgical Sciences, Section of Nuclear Medicine and PET, Uppsala University, Akademiska sjukhuset, 751 85 Uppsala, Sweden. Tel: +46-18-6119644; Fax: +46-18-6110619; E-mail: kerstin.heurling@radiol.uu.se

References

- [1] Klunk WE, Engler H, Nordberg A, Wang Y, Blomqvist G, Holt DP, Bergstro M, Savitcheva I, Debnath ML, Barletta J, Price JC, Sandell

Spectral analysis of ¹⁸F-flutemetamol

- J, Lopresti BJ, Wall A, Koivisto P, Antoni G, Mathis CA, Långstrom B. Imaging Brain Amyloid in Alzheimer's Disease with Pittsburgh Compound-B. *Ann Neurol* 2004; 55: 306-319.
- [2] Thal DR, Rüb U, Orantes M, Braak H. Phases of A β -deposition in the human brain and its relevance for the development of AD. *Neurology* 2002; 58: 1791-1800.
- [3] Vandenberghe R, Van Laere K, Ivanoiu A, Salmon E, Bastin C, Triau E, Hasselbalch S, Law I, Andersen A, Korner A, Minthon L, Garraux G, Nelissen N, Bormans G, Buckley C, Owenius R, Thurfjell L, Farrar G, Brooks DJ. ¹⁸F-flutemetamol amyloid imaging in Alzheimer disease and mild cognitive impairment: a Phase 2 trial. *Ann Neurol* 2010; 68: 319-329.
- [4] Hatashita S, Yamasaki H, Suzuki Y, Tanaka K, Wakebe D, Hayakawa H. [¹⁸F]flutemetamol-amyloid-beta PET imaging compared with [¹¹C]PIB across the spectrum of Alzheimer's disease. *Eur J Nucl Med Mol Imaging* 2014; 41: 290-300.
- [5] Thomas BA, Erlandsson K, Modat M, Thurfjell L, Vandenberghe R, Ourselin S, Hutton B. The importance of appropriate partial volume correction for PET quantification in Alzheimer's disease. *Eur J Nucl Med Mol Imaging* 2011; 38: 1104-1119.
- [6] Sebai S, Baciú M, Ces O, Clarke J, Cunningham V, Gunn R, Law R, Mulet X, Parker C, Plisson C, Templer R, Gee A. To lipophilicity and beyond—towards a deeper understanding of radioligand non-specific binding. *Neuroimage* 2006; 31: T56.
- [7] Fodero-Tavoletti MT, Rowe CC, McLean CA, Leone L, Li QX, Masters CL, Cappai R, Villemagne VL. Characterization of PiB Binding to White Matter in Alzheimer Disease and Other Dementias. *J Nucl Med* 2009; 50: 198-204.
- [8] Veronese M, Bodini B, García-Lorenzo D, Battaglini M, Bongarzone S, Comtat C, Bottlaender M, Stankoff B, Turkheimer FE. Quantification of [¹¹C]PIB PET for imaging myelin in the human brain: a test-retest reproducibility study in high-resolution research tomography. *J Cereb Blood Flow Metab* 2015; [Epub ahead of print].
- [9] Stankoff B, Freeman L, Aigrot MS, Chardain A, Dollé F, Williams A, Galanaud D, Armand L, Lehericy S, Lubetzki C, Zalc B, Bottlaender M. Imaging central nervous system myelin by positron emission tomography in multiple sclerosis using [methyl-¹¹C]-2-(4'-methylamino-phenyl)-6-hydroxybenzothiazole. *Ann Neurol* 2011; 69: 673-680.
- [10] Glodzik L, Rusinek H, Li J, Zhou C, Tsui W, Mosconi L, Li Y, Osorio R, Williams S, Randall C, Spector N, McHugh P, Murray J, Pirraglia E, Vallabhajosula S, de Leon M. Reduced retention of Pittsburgh compound B in white matter lesions. *Eur J Nucl Med Mol Imaging* 2015; 42: 97-102.
- [11] Edison P, Brooks DJ, Turkheimer FE, Archer HA, Hinz R. Strategies for the generation of parametric images of [¹¹C]PIB with plasma input functions considering discriminations and reproducibility. *Neuroimage* 2009; 48: 329-338.
- [12] Nelissen N, Van Laere K, Thurfjell L, Owenius R, Vandenberghe R, Koole M, Bormans G, Brooks DJ, Vandenberghe R. Phase 1 study of the Pittsburgh compound B derivative ¹⁸F-flutemetamol in healthy volunteers and patients with probable Alzheimer disease. *J Nucl Med* 2009; 50: 1251-1259.
- [13] Koole M, Lewis DM, Buckley C, Nelissen N, Vandenberghe R, Brooks DJ, Vandenberghe R, Van Laere K. Whole-body biodistribution and radiation dosimetry of ¹⁸F-GE067: a radioligand for in vivo brain amyloid imaging. *J Nucl Med* 2009; 50: 818-822.
- [14] Curtis C, Gamez JE, Singh U, Sadowsky CH, Villena T, Sabbagh MN, Beach TG, Duara R, Fleisher AS, Frey KA, Walker Z, Hunjan A, Holmes C, Escovar YM, Vera CX, Agronin ME, Ross J, Bozoki A, Akinola M, Shi J, Vandenberghe R, Ikonovic MD, Sherwin PF, Grachev ID, Farrar G, Smith AP, Buckley CJ, McLain R, Salloway S. Phase 3 trial of flutemetamol labeled with radioactive fluorine ¹⁸ imaging and neuritic plaque density. *JAMA Neurol* 2015; 72: 287-294.
- [15] Andersson JL. A Rapid and Accurate Method to Realign PET Scans Utilizing Image Edge Information. *J Nucl Med* 1995; 36: 657-669.
- [16] Svarer C, Madsen K, Hasselbalch SG, Pinborg LH, Haugbøl S, Frøkjær VG, Holm S, Paulson OB, Knudsen GM. MR-based automatic delineation of volumes of interest in human brain PET images using probability maps. *Neuroimage* 2005; 24: 969-979.
- [17] Müller-Gärtner HW, Links JM, Prince JL, Bryan RN, McVeigh E, Leal JP, Davatzikos C, Frost JJ. Measurement of Radiotracer Concentration in Brain Gray Matter Using Positron Emission Tomography: MRI-Based Correction for Partial Volume Effects. *J Cereb Blood Flow Metab* 1992; 12: 571-583.
- [18] Cunningham VJ, Jones T. Spectral Analysis of Dynamic PET Studies. *J Cereb Blood Flow Metab* 1993; 13: 15-23.
- [19] Turkheimer F, Sokoloff L, Bertoldo A, Lucignani G, Reivich M, Jaggi JL, Schmidt K. Estimation of Component and Parameter Distributions in Spectral Analysis. *J Cereb Blood Flow Metab* 1998; 18: 1211-1222.

Spectral analysis of ^{18}F -flutemetamol

- [20] Lammertsma AA, Hume SP. Simplified reference tissue model for PET receptor studies. *Neuroimage* 1996; 4: 153-8.
- [21] Gunn RN, Lammertsma AA, Hume SP, Cunningham VJ. Parametric Imaging of Ligand-Receptor Binding in PET Using a Simplified Reference Region Model. *Neuroimage* 1997; 6: 279-287.
- [22] Heurling K, Buckley C, Van Laere K, Vandenberghe R, Lubberink M. Parametric imaging and quantitative analysis of the PET amyloid ligand ^{18}F -flutemetamol. *Neuroimage* 2015; 121: 184-192.
- [23] Price JC, Klunk WE, Lopresti BJ, Lu X, Hoge JA, Ziolkowski SK, Holt DP, Meltzer CC, DeKosky ST, Mathis CA. Kinetic modeling of amyloid binding in humans using PET imaging and Pittsburgh Compound-B. *J Cereb blood flow Metab* 2005; 25: 1528-1547.
- [24] Turkheimer F, Moresco RM, Lucignani G, Sokoloff L, Fazio F, Schmidt K. The Use of Spectral Analysis to Determine Regional Cerebral Glucose Utilization with Positron Emission Tomography and [^{18}F]Fluorodeoxyglucose: Theory, Implementation, and Optimization Procedures. *J Cereb Blood Flow Metab* 1994; 14: 406-422.